High-energy transitions of shallow magnetodonors in a GaAs/$Al_{0.3}Ga_{0.7}As$ multiple quantum well

2001 J. Phys.: Condens. Matter 13 9761

(http://iopscience.iop.org/0953-8984/13/43/307)

INSTITUTE OF PHYSICS PUBLISHING JOURNAL OF PHYSICS: CONDENSED MATTER

J. Phys.: Condens. Matter **13** (2001) 9761–9772 PII: S0953-8984(01)27946-6

High-energy transitions of shallow magnetodonors in a GaAs/$Al_{0.3}Ga_{0.7}As$ multiple quantum well

A Bruno-Alfonso[1], G-Q Hai[2], F M Peeters[3], T Yeo[4], S R Ryu[4] and B D McCombe[4]

[1] Departamento de Matemática, Faculdade de Ciências, Universidade Estadual Paulista, 17033-360 Bauru, SP, Brazil
[2] Instituto de Física de São Carlos, Universidade de São Paulo, 13560-970 São Carlos, SP, Brazil
[3] Departement Natuurkunde, Universiteit Antwerpen (UIA), B-2610, Antwerpen, Belgium
[4] Department of Physics and Astronomy, State University of New York at Buffalo, Buffalo, NY 14260, USA

Received 16 August 2001
Published 12 October 2001
Online at stacks.iop.org/JPhysCM/13/9761

Abstract

The high-energy states of a shallow donor in a GaAs/$Ga_{0.7}Al_{0.3}As$ multiple-quantum-well structure subjected to a magnetic field in the growth direction are studied both theoretically and experimentally. Effects due to higher confinement subbands as well as due to the electron–phonon interaction are investigated. We show that most of the peaks in the infrared photoconductivity spectrum are due to direct transitions from the ground state to the $m = \pm 1$ magnetodonor states associated with the first subband, but transitions to the $m = \pm 1$ states of the third subband are also apparent. The remaining photoconductivity peaks are explained by *phonon-assisted impurity transitions*.

1. Introduction

Within the effective-mass theory, the problem of a shallow donor in semiconductors is equivalent to that of a hydrogen atom but with very different energy and length scales. In the semiconductor GaAs, e.g., the effective Bohr radius $a_B^* = 0.529\,\epsilon_r m_0/m^*$ Å and effective Rydberg $R^* = 13.6\,m^*/m_0\epsilon_r^2$ eV are about 100 Å and 5.8 meV, respectively. However, exact solutions for shallow impurity states in the presence of magnetic fields are not available. Most theoretical studies on shallow impurities use a variational approach [1]. Other approximate methods such as the perturbation approach [2] and numerical solution of the Schrödinger equation [3, 4] have also been developed.

Different experimental techniques have been used in the study of shallow impurity states in the presence of a magnetic field. Most of the published work has concentrated on the low-energy hydrogen-like transitions [1, 5–7] such as 1s to $2p^{1\pm}$. However, the spectrum contains additional lines at high energies in the presence of a magnetic field. Although these lines are much weaker than those for the 1s-to-$2p^{1\pm}$ transitions, they have been detected by infrared

photoconductivity (IR-PC) measurements for semiconductor materials such as InSb [8, 9]. These transitions arise from the so-called metastable states in a magnetic field as discussed in references [10–12]. They have no hydrogenic counterpart and do not exist in the low-magnetic-field limit either. Although such states are expected to be similar to the Landau states of free electrons, their properties are not well known. Nevertheless, a correspondence between the low-magnetic-field and the high-magnetic-field states has already been established [7]. The terminology 'metastable state' is taken from the problem of shallow donors in bulk material in finite magnetic fields. They are the states with Landau quantum number $N \geqslant 1$ and magnetic quantum number $m < N$ arising from the coupling of the electron motion in the longitudinal and transverse directions. Because $m < N$, the metastable state couples to the continuum spectrum of the lower Landau state through the Coulomb interaction. Such a coupling vanishes at infinite magnetic fields and the metastable states become truly bound [10]. For quasi-2D systems there is no continuum because a perpendicular magnetic field fully quantizes the electron motion. The higher-energy states of a shallow donor in GaAs multiple quantum wells (MQW) were identified by Cheng and McCombe [7] and Dunn *et al* [12]. In their work, the absorption due to the $1s \rightarrow 3p^{1+}$ and $4p^{1+}$ transitions was studied at relatively high energy up to 300 cm^{-1}. Larsen [13] studied theoretically the excited states of magnetodonors in an infinite-barrier quantum well. He also reported anticrossings of magnetodonor levels with the same magnetic number and same symmetry in the growth direction, which are associated with different electric subbands.

Gallium arsenide is a weakly polar semiconductor and as a consequence the shallow impurity states are influenced by the polarization of the material, which is mainly carried by the LO phonons. The electron–LO-phonon interaction affects the shallow donors in the following ways [1, 14–17]: (i) electron–LO-phonon coupling enhances the binding energy of impurity states; (ii) resonances take place when the energy difference between two donor levels equals the LO-phonon energy ($\hbar\omega_{LO} = 297$ cm^{-1} in GaAs); and (iii) phonon-assisted cyclotron resonance harmonics (PACRH) appear on the high-energy side of the absorption spectrum. The first two effects have been studied in detail by Shi *et al* [1]. In their work, the 1s, 2s, $2p^{1\pm}$, $2p_z$, $3d^{2\pm}$, and $4f^{3\pm}$ states were studied in bulk GaAs and GaAs/AlGaAs superlattices. In particular, the effect of the magnetopolaron resonance on the $1s \rightarrow 2p^{1+}$ transition was studied in great detail, and very nice agreement with the experimental results was obtained. The resonant polaron effects on impurity metastable states in GaAs were also observed by van der Sluijs *et al* [10]. Barmby *et al* [11] studied, both experimentally and theoretically, the magnetopolaron resonances of the $m = 1$ states associated with the Landau levels $N = 3$ and 4 ($3p^{1+}$ and $4p^{1+}$, respectively) in n-GaAs. Magnetopolaron splitting was observed for these two metastable states at a transition energy close to the LO-phonon energy.

On the other hand, PACRH were predicted for free electrons by Bass and Levinson [15] and were confirmed experimentally by McCombe *et al* [16] in InSb more than thirty years ago. The PACRH occur when electron transitions between two Landau levels due to the absorption of a photon are accompanied by the absorption or emission of LO phonons. In other words, inelastic LO-phonon scattering is involved in such processes. Phonon-assisted CR harmonics have been studied extensively for free electrons in InSb [15], whereas phonon-assisted impurity transitions (PAIT) were observed much later. Littler *et al* [8] observed experimentally optical transitions between magnetodonor states (associated with Landau levels up to $N = 13$) assisted by the emission of LO phonons. In their theoretical analysis, however, the donor transition energies were obtained from the variational binding energy of the states with $N = 0$ and $m = 1, 2, 3, \ldots$. In the present work we found that the shallow donor states associated with the same high-index Landau subband have almost the same energy, but transitions from the 1s-like ground state to $m = +1$ states dominate the far-infrared absorption at low temperature.

This work is devoted to the theoretical and experimental study of the high-energy transitions of a shallow donor and their interaction with LO phonons in GaAs/$Al_{0.3}Ga_{0.7}As$ multiple quantum wells in the presence of a perpendicular magnetic field. We present in section 2 our calculations of the shallow donor states in the presence of a perpendicular magnetic field. We adapted the high-field method proposed by Barmby *et al* [3] for shallow donor states in a three-dimensional system to our MQW system. The magneto-optical experiment is described in section 3, while the far-infrared absorption due to direct transitions of shallow donors and the effects of the higher MQW subbands are presented in section 4. The phonon-assisted impurity transitions are investigated in section 5. We summarize our results in section 6.

2. Shallow donor states in multiple quantum wells in perpendicular magnetic fields

We consider a periodic GaAs/$Ga_{0.7}Al_{0.3}As$ multiple-quantum-well structure with well and barrier thicknesses $d_w = 200$ Å and $d_b = 100$ Å, respectively, in the presence of a uniform magnetic field $\vec{B}$ applied in the growth direction (the z-axis). The Hamiltonian of a single hydrogenic donor impurity in the system is written as

$$\hat{H} = \frac{1}{2}(-\mathrm{i}\hbar\vec{\nabla} + e\vec{A}) \cdot \frac{1}{m^*(z)}(-\mathrm{i}\hbar\vec{\nabla} + e\vec{A}) + V_{SL}(z) - \frac{e^2}{4\pi\epsilon_0\epsilon_r|\vec{r}-\vec{r}_i|} \tag{1}$$

where $V_{SL}(z)$ is the MQW confinement potential with conduction band offset $V_0 = 224.5$ meV, $m^*(z)$ the position-dependent effective mass ($m^* = m_w^* = 0.067\ m_0$ in the well and $m^* = m_b^* = 0.092\ m_0$ in the barrier), $\vec{A}$ the magnetic vector potential, $\vec{r}_i = (0, 0, z_i)$ the impurity position, and $\epsilon_r = 12.5$ the average dielectric constant.

The wavefunctions are chosen as eigenfunctions of angular momentum $\hat{L}_z$ in the z-direction, i.e.,

$$\Psi_m(\vec{r}) = \frac{\mathrm{e}^{\mathrm{i}m\varphi}}{\sqrt{2\pi}}\Phi_m(\rho, z) \qquad m = 0, \pm1, \pm2, \ldots \tag{2}$$

where $\Phi_m(\rho, z)$ is an eigenfunction of

$$\hat{H}_m = -\frac{\hbar^2}{2}\frac{\partial}{\partial z}\frac{1}{m^*(z)}\frac{\partial}{\partial z} + \frac{\hbar^2}{2m^*(z)}\left[-\frac{1}{\rho}\frac{\partial}{\partial\rho}\left(\rho\frac{\partial}{\partial\rho}\right) + \frac{m^2}{\rho^2} + \frac{m}{\lambda_B^2} + \frac{\rho^2}{4\lambda_B^2}\right] + V_{SL}(z) - \frac{e^2}{4\pi\epsilon_0\epsilon_r|\vec{r}-\vec{r}_i|} \tag{3}$$

with $\vec{A} = B\rho\hat{\varphi}/2$, where have we made use of cylindrical coordinates (ρ, φ, z), and $\lambda_B = \sqrt{\hbar/(eB)}$ is the cyclotron radius. The function $\Phi_m(\rho, z)$ is calculated by adapting the high-field method of Barmby *et al* [3], as described below.

First, we look for separable solutions of $\hat{H}_m\Phi_m = E_m\Phi_m$ in the form $\tilde{\Phi}_{n,m}(\rho, z) = R_{n,m}(\rho)\psi_{n,m}(z)$, with

$$R_{n,m}(\rho) = \frac{1}{\lambda_B}\sqrt{\frac{n!}{(n+|m|)!}}\left(\frac{\rho}{\lambda_B\sqrt{2}}\right)^{|m|}\exp\left(-\frac{\rho^2}{4\lambda_B^2}\right)L_n^{|m|}\left(\frac{\rho^2}{2\lambda_B^2}\right) \qquad n = 0, 1, 2, \ldots \tag{4}$$

where $L_n^{|m|}$ is a Laguerre polynomial. The best choice for $\psi_{n,m}(z)$ satisfies $\hat{H}_{n,m}\psi_{n,m} = \tilde{E}_{n,m}\psi_{n,m}$ with

$$\hat{H}_{n,m} = -\frac{\hbar^2}{2}\frac{\partial}{\partial z}\frac{1}{m^*(z)}\frac{\partial}{\partial z} + \frac{\hbar^2}{2m^*(z)}\left(\frac{2n+m+|m|+1}{\lambda_B^2}\right) + V_{SL}(z) + V_{n,m}(z) \tag{5}$$

where

$$V_{n,m}(z) = -\frac{e^2}{4\pi\epsilon_0\epsilon_r}\langle R_{n,m}(\rho)|[1/\sqrt{\rho^2+(z-z_i)^2}]|R_{n,m}(\rho)\rangle \tag{6}$$

is the effective Coulomb potential in the z-direction.

Because we are interested in bound impurity states, the artificial boundary condition $\psi_{n,m}(z_i \pm L/2) = 0$ is imposed for sufficiently large L. Instead of determining $\psi_{n,m}(z)$ by a finite-difference calculation and deriving analytical expressions after a Fourier-transformation procedure [3], we choose to directly obtain the Fourier coefficients by diagonalization of the matrix representation of $\hat{H}_{n,m}$ in the trigonometric basis. The solutions obtained:

$$\psi_{n,m,\nu}(z) = \sqrt{\frac{2}{L}}\sum_k c_k^{(n,m,\nu)} \sin\left(k\pi\left[\frac{z-z_i}{L}+\frac{1}{2}\right]\right) \qquad k = 1, 2, \ldots \tag{7}$$

with the corresponding energies $\tilde{E}_{n,m,\nu}(\nu = 1, 2, \ldots)$ are appropriate for Φ_m and $E_{n,m}$ at high magnetic fields, for which the electron motions in the xy-plane and in the z-direction are essentially separate. For intermediate magnetic fields the coupling between such modes is taken into account as follows:

$$\Phi_m(\rho, z) = \sum_{n,\nu} a_{n,\nu}^{(m)}\tilde{\Phi}_{n,m,\nu}(\rho, z) = \sum_{n,\nu} a_{n,\nu}^{(m)} R_{n,m}(\rho)\psi_{n,m,\nu}(z) \tag{8}$$

where the coefficients $a_{n,\nu}^{(m)}$ and the energy E_m satisfy

$$\sum_{n',\nu'}\langle R_{n,m}(\rho)\psi_{n,m,\nu}(z)|\hat{H}_m|R_{n',m}(\rho)\psi_{n',m,\nu'}(z)\rangle a_{n',\nu'}^{(m)} = E_m a_{n,\nu}^{(m)}. \tag{9}$$

After diagonalization of the above eigensystem a set of solutions $\Phi_{m,\mu}(\rho, z)$, i.e. the coefficients $a_{n,\nu}^{(m,\mu)}$, with corresponding energies $E_{m,\mu}$ $(\mu = 1, 2, \ldots)$, are obtained. The three-dimensional wavefunction is $\Psi_{m,\mu}(\vec{r}) = \Phi_{m,\mu}(\rho, z)\ \mathrm{e}^{\mathrm{i}m\varphi}/\sqrt{2\pi}$, in agreement with equation (2). In the calculation, the convergence of our numerical results is checked by varying L, the dimension of the Fourier basis, and the range of n. The index ν merits a separate discussion. For a given radial mode $R_{n,m}$, each longitudinal mode $\psi_{n,m,\nu}$ may be associated with a MQW subband. Some longitudinal modes, called on-site modes, are essentially localized in the quantum well (QW) which contains the donor, while most $\psi_{n,m,\nu}$, called off-site or remote modes, are reminiscent of the extended Bloch states in the MQW. For simplicity, we limit our calculations to on-site modes, which should be more strongly coupled (via photons or phonons) to the 1s-like ground state. As for each MQW subband j $(j = 1, 2, \ldots)$ with n and m given there is one on-site mode only, on-site longitudinal modes are labelled from now on with j instead of ν. Additionally, to aid the understanding of the theoretical results, the index μ will be replaced by the pair (N, j) which maximizes $|a_{n,j}^{(m,\mu)}|^2$, with $N = n + (m + |m|)/2$. In this way, magnetodonor states are denoted as (N, m, j) with corresponding energy levels $E_{N,m,j}$, where N stands for the Landau level with which the impurity state is associated.

In correspondence with the experimental situation (to be presented below), the numerical calculation is applied to a single donor impurity at the centre of a well (chosen at $z = 0$). This additional symmetry allows the separation of impurity states according to their parity with respect to the $z = z_i = 0$ plane. That is, the on-site modes are even (odd) for $j = 1$ and $j = 3$ $(j = 2)$. We consider 16 periods of the MQW in which we confirm that the impurity states under study are localized. In the Fourier expansion, we include up to 400 harmonics and incorporate on-site modes only. The impurity levels below the $N = 20$ Landau level of the first subband are calculated for each m, including radial modes with $n = 0, 1, \ldots, 25$.

Figure 1 shows the impurity energy levels $E_{N,0,j}$, with $N = 0, 1, \ldots, 10$ and $j = 1, \ldots, 3$, as functions of magnetic field strength. Three fans of magnetodonor states are present, each

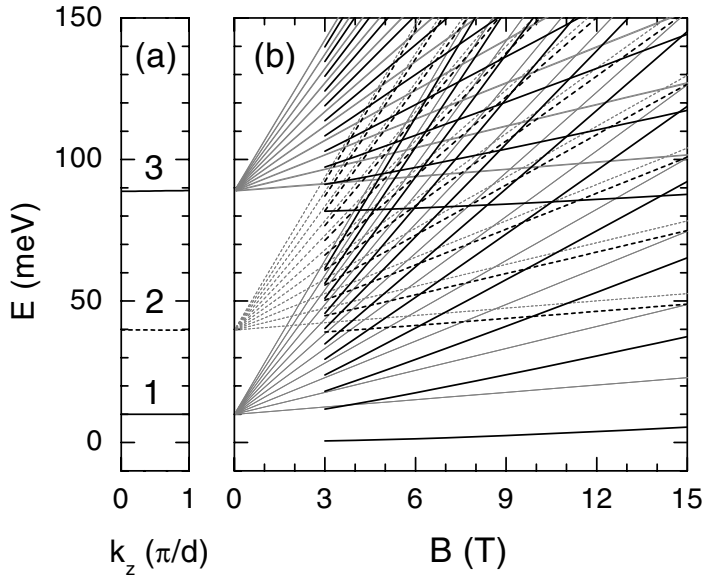

Figure 1. (a) The lower MQW electric subbands as functions of the Bloch wavenumber k_z (in units of π/d, where $d = 300$ Å is the MQW period). (b) The magnetodonor energy levels $E_{N,0,j}$ for $N = 1, \ldots, 10$ and $j = 1, 2, 3$ as functions of the magnetic field strength (thick black lines) in the MQW. The corresponding Landau levels are also shown as thin grey lines. Levels for $j = 1, 3$ ($j = 2$) are plotted as solid (dashed) curves.

one corresponding to a MQW subband. For comparison, the free-electron Landau levels of the first three subbands are also shown in the figure. Levels for $j = 1, 3$ ($j = 2$) are plotted as solid (dashed) curves. As discussed above, impurity states for $j = 1, 3$ ($j = 2$) are even (odd) in the z-direction. The ground magnetodonor state is $(0, 0, 1)$, and often called 1s-like. This state is associated with the Landau level $N = 0$ and the MQW subband $j = 1$, and is even in the z-direction. The difference between a bound impurity state and its corresponding Landau level lies in the binding energy of the state. Clearly, this binding energy decreases with increasing Landau quantum number.

We also found that the states $(N', 0, 3)$ of the third subband couple to those, $(N, 0, 1)$, of the first subband, resulting in anticrossings of magnetodonor levels [13] (not shown in figure 1). Such a coupling occurs between magnetodonor states with the same parity in the z-direction, and is due to the Coulomb term in the Hamiltonian $\hat{H}_m$ (see equation (3)). However, we simplified the present study by disregarding the relatively small coupling between separate solutions $\tilde{\Phi}_{n,m,j}(\rho, z)$ with $j = 1$ and $j = 3$. On one hand, this simplification makes the discussion easier. On the other hand, the effects of such a coupling are not apparent in our experimental results, so they do not merit further attention in this report.

3. Experiment

Extensive far-infrared magneto-optical studies have been carried out on GaAs/$Al_{0.3}Ga_{0.7}As$ multiple-quantum-well (MQW) samples to explore PAIT and PACR transitions, as well as direct transitions to high-energy impurity states. Magneto-photoconductivity and far-infrared magneto-transmission measurements were employed. Results obtained with the former technique are the main focus of this paper, but it is worth mentioning that PAIT and PACR

transitions were not detected by far-infrared transmission studies on a wide range of quantum well samples with different impurity and electron densities. From the latter measurement the intensity of the PACR is estimated to be much less than 1% of the cyclotron resonance (CR), much smaller than the earlier-predicted values (about 10%) [18, 19]. Extensive FIR-PC experiments were performed on a GaAs/$Al_{0.3}Ga_{0.7}As$ MQW sample, δ-doped with Si in the well centre to a nominal density of 2×10^{10} cm^{-2}. The sample contains 50 periods of 200 Å wells and 100 Å barriers and was grown by molecular beam epitaxy. Two ohmic contacts were fabricated on a 6×6 mm^2 piece of the sample by indium diffusion. The FIR-PC experiments were performed with a CO_2 laser in conjunction with a 17 T superconducting magnet system, light pipe, and condensing cone optics. Special care was taken to orient the sample-growth direction parallel to the magnetic field to eliminate the influence of subband–Landau-level coupling due to the in-plane magnetic field. The sample was cooled to liquid-helium temperature in the dark. While chopping the FIR laser light at ~200 Hz with constant current (~1 μA) between the two ohmic contacts, the voltage change between these contacts was monitored as a function of magnetic field by phase-sensitive lock-in detection. The wavelength range studied was 9.7 μm–10.7 μm.

4. Optical absorption due to direct transitions

As described above, magneto-photoconductivity spectra were measured for a lightly doped sample at liquid-He temperature under linearly polarized infrared laser irradiation in the Faraday configuration. In these conditions, the impurity magneto-optical absorption due to direct transitions consists of $(0, 0, 1) \rightarrow (N, \pm 1, j)$ transitions, according to the selection rule $\Delta m = \pm 1$. The symmetry in the z-direction (isolated donor at the centre of a QW) leads to an additional parity selection rule. Namely, for direct transitions from the 1s-like ground state $(0, 0, 1)$, which is even in the z-direction, the final state should also be even. Therefore, in this section, we are mainly interested in even magnetodonor states.

In figure 2 we show the impurity levels associated with $(N, -1, j)$ and $(N, 1, j)$ states, as dashed and solid lines, respectively. The ground 1s-like level $E_{0,0,1}$ is indicated by the dotted line. Only even states with $j = 1$ or $j = 3$ are shown, according to the parity selection rule in the z-direction. Note that transitions to even states for $j = 2$ are essentially forbidden, as those states correspond to off-site longitudinal modes. The lowest $m = 1$ state $(1, 1, 1)$, called the $2p^{1+}$-like state in the usual spectroscopic notation, is associated with the $N = 1$ Landau level. In the same way, the lowest $m = -1$ state $(0, -1, 1)$, i.e., the $2p^{1-}$-like state, is associated with the lowest Landau level $N = 0$. It is also found that $(N, 1, j)$ and $(N, -1, j)$ states are almost degenerate for $N \geqslant 1$. However, the optical absorption due to direct transitions for light frequencies is dominated by the transitions to $(N, 1, j)$ states, as will be shown below.

The absorption coefficient may be calculated by perturbation theory. For the transition $(0, 0, 1) \rightarrow (N, \pm 1, j)$ the oscillator strength is given by

$$T_{N,\pm 1,j} = \frac{E_{N,\pm 1,j} - E_{0,0,1}}{\hbar\omega_c} |\langle N, \pm 1, j|[\rho/(\lambda_B\sqrt{2})]|0, 0, 1\rangle|^2 \tag{10}$$

where

$$\langle N, \pm 1, j|[\rho/(\lambda_B\sqrt{2})]|0, 0, 1\rangle = \sum_{n', j', k} \sqrt{n'+1}\, a_{n', \nu'}^{(N,\pm 1, j)} c_k^{(n', \pm 1, j')} \times \sum_{j''} \left(a_{n', j''}^{(0,0,1)} c_k^{(n', 0, j'')} - a_{n'+1, j''}^{(0,0,1)} c_k^{(n'+1, 0, j'')} \right) \tag{11}$$

and $\omega_c = eB/m_w^*$.

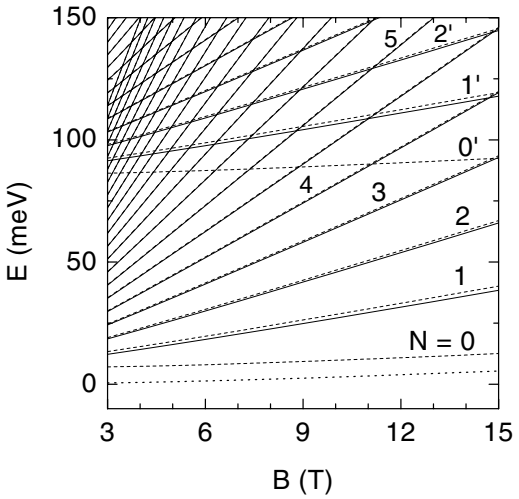

Figure 2. The magnetodonor energy levels $E_{N,1,j}$ (solid curves) and states $E_{N,-1,j}$ (dashed curves) for $j = 1$ (lower fan) and $j = 3$ (upper fan), as functions of magnetic field strength B (in T). The 1s-like ground state $E_{0,0,1}$ is given by the dotted curve.

The calculated oscillator strengths are displayed in figure 3 for direct transitions as a function of the magnetic field strength B from (0, 0, 1) to: (a) $(N, 1, 1)$ with $N = 1, \ldots, 20$; (b) $(N, -1, 1)$ with $N = 0, \ldots, 20$; (c) $(N, 1, 3)$ with $N = 1, \ldots, 10$; and (d) $(N, -1, 3)$ with $N = 0, \ldots, 10$. As may be noted, with increasing N, the absorption strength decreases monotonically. For B between 3 T and 15 T, the oscillator strength $T_{1,1,1}$ for the $2p^{1+}$-like state varies from $1/2$ to $4/5$, whereas $T_{0,-1,1}$, which is associated with the $2p^{1-}$-like state, goes

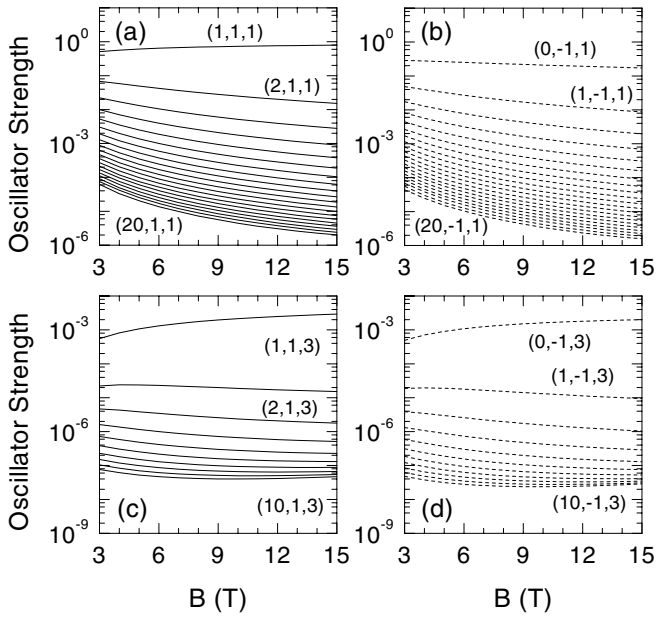

Figure 3. The theoretical oscillator strengths for direct transitions from (0, 0, 1) to: (a) $(N, 1, 1)$ with $N = 1, \ldots, 20$; (b) $(N, -1, 1)$ with $N = 0, \ldots, 20$; (c) $(N, 1, 3)$ with $N = 1, \ldots, 10$; and (d) $(N, -1, 3)$ with $N = 0, \ldots, 10$, as functions of the magnetic field strength B. As in figure 2, solid (dashed) curves are for $m = 1$ ($m = -1$) states.

from 1/3 to 1/6. Also, the ratio $T_{N,1,1}/T_{N,-1,1}$ between the oscillator strengths for almost degenerate states of the first subband is: 10–100, 4–8, 2–4 and 1–2 for $N = 1$, $N = 2$, $N = 3, 4, 5$, and $N = 6, \ldots, 20$, respectively (see figures 3(a), 3(b)). In the same way, the ratio $T_{N,1,3}/T_{N,-1,3}$ for the third subband is: 30–300, 5–15, 2–5, and 3/2–2 for $N = 1$, $N = 2$, $N = 3, \ldots, 7$, and $N = 8, 9, 10$, respectively (see figures 3(c), 3(d)). Hence, we conclude that the optical absorption due to direct transitions for light frequencies around such (almost) degenerate levels is dominated by transitions to the $(N, 1, j)$ states. This behaviour is stronger for lower Landau levels. On the other hand, direct transitions to $(0, -1, j)$ states, which are not degenerate with $m = 1$ states, should be apparent in infrared magneto-optical absorption spectra.

Furthermore, as may be noted in figure 3, the transitions to $(N, \pm 1, 3)$ magnetodonor states are in general weaker than those to $(N, \pm 1, 1)$ states. However, such a comparison should be applied to neighbouring levels. In this respect, the $E_{1,1,3}$-level crosses $E_{N,\pm 1,1}$-levels for $N \geqslant 3$ and $B < 15$ T. At the same time, the oscillator strengths satisfy $T_{1,1,3} \gtrsim T_{N,\pm 1,1}$ whenever $E_{N,\pm 1,1} < E_{1,1,3} < E_{N+1,\pm 1,1}$. The same arguments apply to the direct transition $(0, 0, 1) \rightarrow (0, -1, 3)$. Hence, transitions from the 1s-like state to $(1, 1, 3)$ and $(0, -1, 3)$ states should be apparent in the infrared magneto-optical spectrum. Unfortunately, the corresponding wavelengths were not available in our experimental set-up. Other transitions to magnetodonor states associated with the third electric subband may also appear in the absorption spectrum, but as secondary or shoulder structures only.

The theoretical transition energies $E_{N,\pm 1,j} - E_{0,0,1}$ are shown in figure 4 for $N = 0, 1, \ldots, 20$ and $j = 1, 3$ in the range of laser frequencies used in the experiment. Solid (dashed) lines are for $m = 1$ ($m = -1$), and steeper (less steep) lines are for $j = 1$ ($j = 3$). Circles represent the peak positions in the measured photoconductivity spectrum for each laser wavelength. For convenience of discussion, some of the experimental data are indicated by open symbols. The dash–dotted (for $m = 1$, $j = 1$) and dash–dot–dotted (for $m = -1$, $j = 1$) lines, which correspond to phonon-assisted impurity transitions, are discussed in section 5.

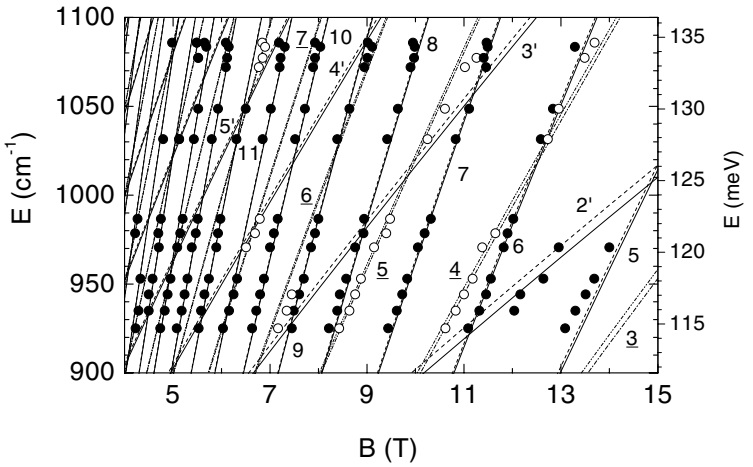

Figure 4. Theoretical transition energies $E_{N,\pm 1,j} - E_{0,0,1}$ for direct transitions with $N = 0, 1, \ldots, 20$ and $j = 1, 3$ as functions of the magnetic field strength B. Solid (dashed) lines are for $m = 1$ ($m = -1$). Steeper (less steep) lines labelled by N (N') are for $j = 1$ ($j = 3$), where N (N') is the Landau-level index. The experimental data are given by the symbols. Dash–dotted (for $m = 1$, $j = 1$) and dash–dot–dotted (for $m = -1$, $j = 1$) lines, labelled by $\underline{N}$, are for phonon-assisted impurity transitions with energies $\hbar\omega_{LO} + E_{\underline{N},\pm 1,j} - E_{0,0,1}$.

In the theoretical results, the conduction band non-parabolicity is taken into account by adding the fourth-order term [20]

$$\hat{W} = \eta\left(-i\vec{\nabla} + \frac{e}{\hbar}\vec{A}\right)^4 \tag{12}$$

to the Hamiltonian in equation (1), where [21] $\eta = -2107$ eV Å^4 for GaAs. Then, using first-order perturbation theory, the magnetodonor level $E_{N,m,j}$ is corrected by adding the quantity

$$\langle N, m, j|\hat{W}|N, m, j\rangle = \eta \sum_{k,n',j',j''} a_{n',j'}^{(N,m,j)} a_{n',j''}^{(N,m,j)} c_k^{(n',m,j')} c_k^{(n',m,j'')} \times \left(\frac{2n' + m + |m| + 1}{\lambda_B^2} + \frac{k^2\pi^2}{L^2}\right)^2. \tag{13}$$

It is important to stress that for free-electron Landau levels such a procedure leads to essentially the same results as the formula proposed by Ruf and Cardona [22, 23], with a typical non-parabolicity parameter $C^* = -3.0$ for GaAs.

In figure 4 we observe that:

(i) most of the experimental data are nicely recovered by the theoretical results for the direct transitions associated with the first confinement subband $j = 1$ (the set of steepest lines);
(ii) some experimental data may be explained by direct transitions to the $j = 3$ subband (the set of less steep curves);
(iii) the weak anticrossings between magnetodonor levels of $j = 1$ and $j = 3$ subbands (not shown) are not apparent in the experimental data; and
(iv) there are experimental points (for instance, the open circles at high energy) which do not correspond to any direct transition.

It should be stressed that magnetopolaron corrections due to electron–LO-phonon interaction may account for small energy differences in the figure. Figure 5 displays the experimental IR-PC spectrum for laser wavelengths (a) $\lambda = 10.494$ μm and (b) $\lambda = 10.135$ μm, after removing the background, on a logarithmic scale. The positions of the peaks in the experimental spectra correspond to symbols in figure 4 at photon energies (a) 952.93 cm^{-1} (118.15 meV) and (b) 986.68 cm^{-1} (122.33 meV), respectively. The corresponding theoretical absorption spectra (dot–dashed curves) associated with direct transitions to $(N, \pm 1, j)$ states are also shown in figure 5. The four lower curves in figures 5(a) and 5(b) represent the contributions of $(N, 1, 1)$, $(N, -1, 1)$, $(N, 1, 3)$, and $(N, -1, 3)$ states to the optical absorption, where a Lorentzian lineshape was used for all the different transitions. To simulate the mean broadening of the peaks in the experimental IR-PC signal, line-broadening values of 58.1 cm^{-1} (7.2 meV) and 14.5 cm^{-1} (1.8 meV) were taken for $j = 1$ and $j = 3$, respectively. Again, it is clear in the figures that transitions to $(N, 1, 1)$ states dominate the optical absorption due to direct transitions.

In figure 5(a) one may note that the theoretical optical absorption spectrum resembles the experimental IR-PC signal for $\lambda = 10.494$ μm. In particular, the shoulder in the experimental spectrum at about 12.6 T (see the double arrow in figure 5(a)) may be explained by a direct transition to the (2, 1, 3) magnetodonor state. The main difference between the spectra is an extra peak at about 8.9 T (indicated by the single arrow in figure 5(a)) in the IR-PC signal, which is associated with an open circle in figure 4. As is apparent in figure 5(a), such a peak does not correspond to a direct transition. Instead, it may be explained if the electron–LO-phonon interaction is included, as will be discussed below.

As shown in figure 5(b), as well as in figure 4 for the corresponding peak positions at photon energy 986.68 cm^{-1}, the agreement between the experimental IR-PC and the calculated

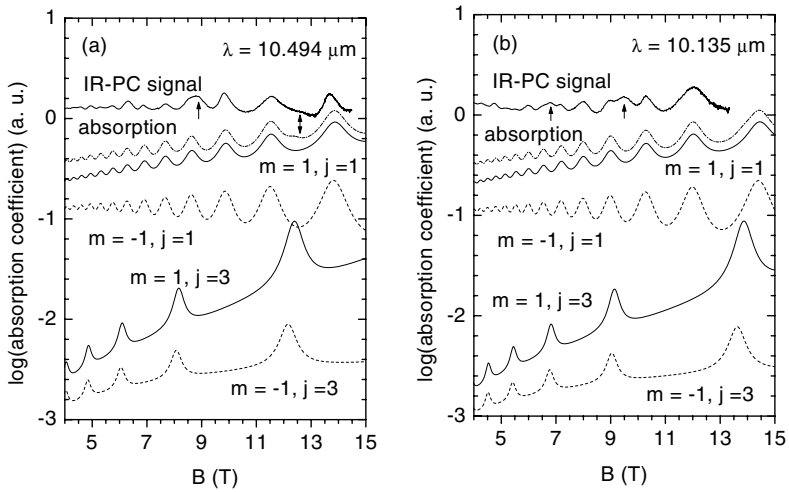

Figure 5. The theoretical absorption spectrum due to direct transitions (dot–dashed curve) from the ground state to $(N, \pm 1, j)$ states, and the IR-PC signal (upper curve) at laser wavelengths (a) $\lambda = 10.494\ \mu$m and (b) $\lambda = 10.135\ \mu$m. The four lower curves represent the contributions of $(N, 1, 1)$, $(N, -1, 1)$, $(N, 1, 3)$, and $(N, -1, 3)$ states to the optical absorption.

optical absorption is reasonable, except for the two peaks at $B = 6.8$ T and $B = 9.5$ T in the IR-PC signal. Such peaks are indicated by arrows in figure 5(b) and correspond to open circles in figure 4. The peak at 9.5 T is far from the resonance energies for direct transitions, while that at 6.8 T is at about the transition energy to $(4, \pm 1, 3)$ states of the third subband. However, such peaks are stronger than neighbouring peaks corresponding to the first electric subband. Consequently, those additional peaks may be explained not by direct transitions but by phonon-assisted impurity transitions, which will be discussed in the next section. Transitions to the magnetodonor states of the third subband are not apparent in the IR-PC spectrum for $\lambda = 10.135\ \mu$m.

5. Phonon-assisted impurity transitions

We have shown in the previous section that a small number of the peaks observed in the magneto-optical absorption cannot result from the direct transitions. The only possible way to explain the additional absorption lines in the present experiment is through phonon-assisted impurity transitions. It is well known that the electron–phonon interaction and the magneto-polaron effects play important roles in the magneto-optical absorption spectrum of polar semiconductors. The magnetopolaron resonance results in an energy splitting [1, 24, 25]. The phonon-assisted harmonics lead to the so-called phonon-assisted absorption on the high-frequency side [15]. Initially forbidden transitions are possible when electron–phonon interaction is included, because it involves inelastic scattering which breaks the selection rules for the direct transition.

Figure 4 shows the transition energy of the LO-phonon-mediated, i.e. indirect, transitions. Dash–dotted (dash–dot–dotted) lines are for electronic transitions to $(\underline{N}, 1, 1)$ $((\underline{N}, -1, 1))$ magnetodonor states. The underlined label $\underline{N}$ is used in figure 4 to distinguish indirect transitions from direct ones. The phonon-assisted impurity transitions with energies $\hbar\omega_{LO} + E_{\underline{N},m,j} - E_{0,0,1}$ correspond to absorption processes involving the emission of one LO phonon.

In principle, all impurity states are allowed in such transitions. In this sense, we represented transition energies for $m = \pm 1$ only, but other values of m should also be included. In fact, the latter are not explicitly included in figure 4 because magnetodonor levels are almost degenerate in the energy range of the experiment.

An overall agreement of indirect transition energies with the experimental results is apparent in figure 4 (see the open circles). Notice that not all of the theoretically predicted phonon-assisted impurity transitions are seen experimentally. A possible explanation for this arises in figure 5, where for a fixed laser frequency the absorption peaks on the high-magnetic-field side, which correspond to the lower Landau index N, are stronger. The fact that we do not observe the phonon-assisted harmonics close to these strong peaks is probably due to the large linewidth of these direct transitions, as is apparent in figure 5. On the low-magnetic-field side, different transitions are very close to each other, with smaller oscillator strength (i.e. higher N), and therefore they are difficult to observe.

Previously [23], we calculated the PACRH due to free electrons in GaAs/AlGaAs quantum wells for the Landau levels up to $N = 2$ and found a very small oscillator strength for these transitions. This is consistent with the experimental measurements described in section 3, in which such transitions were not observed. In this respect, it is important to stress that although we assumed a close relation between optical absorption and photoconductivity, the corresponding spectra do not necessarily coincide. The oscillator strength of phonon-assisted transitions should be calculated to explain far-infrared magneto-transmission measurements, while a more complicated theory is needed for the magneto-photoconductivity spectra.

6. Summary

We have studied both theoretically and experimentally the shallow donor states in a GaAs/$Ga_{0.7}Al_{0.3}As$ multiple-quantum-well structure, with well width $d_w = 200$ Å and barrier width $d_b = 100$ Å, in the presence of a perpendicular magnetic field. The impurity states were calculated by adapting a numerical method previously reported for bulk states. Special attention was paid to the high-energy impurity states and the associated magneto-optical absorption spectrum. Effects of the electron–phonon interaction were considered and discussed. A good overall agreement between theory and experiment was found and magnetopolaron corrections due to electron–LO-phonon interaction may account for small energy differences.

Extensive far-infrared magneto-optical studies have been carried out on the multiple-quantum-well sample. In this system, the energies of the first three subbands are comparable to the experimental excitation energy, and therefore intersubband coupling may also influence the impurity states and the corresponding absorption spectra. We obtained the different donor energy levels associated with 21 Landau levels in the first three electric subbands. The coupling of magnetodonor states of the first and third subbands leads to anticrossings which are not shown, as they are not apparent in the experimental data. We found that for higher Landau levels the $m = -1$ states are almost degenerate with $m = 1$ states, which have larger oscillator strength. We also showed that direct transitions from the ground state to the $m = 1$ states of the first electric subband dominate the absorption spectra, although transitions to $m = \pm 1$ states of the third subband may be apparent. In this respect, clear experimental evidence is found in the IR-PC spectrum for the intersubband transitions $(0, 0, 1) \rightarrow (2, 1, 3)$.

Beyond the absorption due to the direct transitions, the additional absorption peaks are explained by phonon-assisted impurity transitions, since the corresponding transition energies are in good agreement with the experimental data. In such indirect transitions the selection rule $\Delta m = \pm 1$ for the angular momentum m breaks down and, in principle, all magnetodonor states can lead to phonon-assisted impurity transitions. Furthermore, we found that at high energy,

magnetodonor states for different values of m which are associated with the same Landau level have very close energies. Therefore, although more transition channels are allowed for the phonon-assisted transition, it should be difficult to resolve them in the experimentally observed IR-PC peaks. Calculations of magnetopolaron effects and oscillator strengths for phonon-assisted transitions are in progress.

Acknowledgments

This work was partially supported by FAPESP and CNPq (Brazil), the Flemish Science Foundation, the 'Bijzonder onderzoeksfonds van de Universiteit Antwerpen', and IUAP (Belgium). ABA is grateful for hospitality at IF-USP where part of this work began. Part of this work was completed when GQH was a visitor at the University of Antwerp (UIA). Work at the University of Buffalo was supported in part by ONR.

References

[1] Shi J M, Peeters F M and Devreese J T 1993 *Phys. Rev.* B **48** 5202
Shi J M, Peeters F M and Devreese J T 1994 *Phys. Rev.* B **50** 15 185
Shi J M, Peeters F M, Hai G Q and Devreese J T 1991 *Phys. Rev.* B **44** 5692
[2] Wetzel C, Meyer B K and Omling P 1993 *Phys. Rev.* B **47** 15 588
Dai C M and Chuu D S 1991 *Physica* B **172** 445
[3] Barmby P W, Dunn J L, Bates C A and Klaassen T O 1998 *Phys. Rev.* B **57** 9286 and references therein
[4] Kuhn T, Mahler G, Dunn J L and Bates C A 1994 *J. Phys.: Condens. Matter* **6** 757
[5] Cheng J-P, McCombe B D, Brozak G and Schaff W 1993 *Phys. Rev.* B **48** 17 243
[6] Allan G R, Black A, Pidgeon C R, Gornik E, Seidenbusch W and Colter P 1985 *Phys. Rev.* B **31** 3560
Latgé A, Porras-Montenegro N and Oliveira L E 1995 *Phys. Rev.* B **51** 2259
Bruno-Alfonso A, de Dios-Leyva M and Oliveira L E 1998 *Phys. Rev.* B **57** 6573
[7] Cheng J-P and McCombe B D 1990 *Phys. Rev.* B **42** 7626
[8] Littler C L, Zawadzki W, Loloee M R, Song X N and Seiler D G 1989 *Phys. Rev. Lett.* **63** 2845
[9] Goodwin M W and Seiler D G 1983 *Phys. Rev.* B **27** 3451
[10] van der Sluijs A J, Geerinck K K, Klaassen T O, Wenckebach W Th and Foxon C T 1994 *J. Appl. Phys.* **75** 3698
[11] Barmby P W, Dunn J L, Bates C A, Pearl E P, Foxon C T, van der Sluijs A J, Geerinck K K, Klaassen T O, van Klarenbosch A and Langerak C J G L 1994 *J. Phys.: Condens. Matter* **6** 7868
[12] Dunn J L and Pearl E 1991 *J. Phys.: Condens. Matter* **3** 8605
Pearl E P, Dunn J L and Bates C A 1992 *J. Phys.: Condens. Matter* **4** L199
[13] Larsen D M 1991 *Phys. Rev.* B **44** 5629
[14] Helm M, Peeters F M, DeRosa F, Colas E, Harbison J P and Florez L T 1991 *Phys. Rev.* B **43** 13 983
[15] Bass F G and Levinson I B 1965 *Zh. Eksp. Teor. Fiz.* **49** 914 (Engl. Transl. 1966 *Sov. Phys.–JETP* **22** 635)
For a review, see
Ivanov-Omskii V I, Korovin L I and Shereghii E M 1978 *Phys. Status Solidi* b **90** 11
Bakanas R K, Bass F G and Levinson I B 1978 *Sov. Phys.–Semicond.* **12** 863
[16] McCombe B D, Bishop S G and Kaplan R 1967 *Phys. Rev. Lett.* **18** 748
McCombe B D and Kaplan R 1968 *Phys. Rev. Lett.* **21** 756
[17] Peeters F M and Devreese J T 1994 *Proc. Nonlinear Physics* ed V D Lakhno (New York: Wiley) p 99
[18] Badalyan S M and Levinson I B 1988 *Sov. Phys.–Semicond.* **22** 1278
[19] Tanatar B and Singh M 1990 *Phys. Rev.* B **42** 3077
[20] Bruno-Alfonso A, Diago-Cisneros L and de Dios-Leyva M 1995 *J. Appl. Phys.* **77** 2837
Braun M and Rössler U 1985 *J. Phys. C: Solid State Phys.* **18** 3365
[21] Lommer G, Malcher F and Rössler U 1986 *Superlatt. Microstruct.* **5** 273
[22] Ruf T and Cardona M 1991 *Phys. Rev.* B **41** 10 747
[23] Hai G Q, Peeters F M, Studart N, Wang Y J and McCombe B D 1998 *Phys. Rev.* B **58** 7822
[24] López V, Comas F, Trallero-Giner C, Ruf T and Cardona M 1996 *Phys. Rev.* B **54** 10 502
[25] Peeters F M and Devreese J T 1985 *Phys. Rev.* B **31** 3689
Peeters F M and Devreese J T 1986 *Phys. Rev.* B **33** 4330